

Maximum mass, moment of inertia and compactness of relativistic stars

Cosima Breu and Luciano Rezzolla

Institute for Theoretical Physics, Max-von-Laue-Str. 1, 60438 Frankfurt, Germany
Frankfurt Institute for Advanced Studies, Ruth-Moufang-Str. 1, 60438 Frankfurt, Germany

12 April 2016

ABSTRACT

A number of recent works have highlighted that it is possible to express the properties of general-relativistic stellar equilibrium configurations in terms of functions that do not depend on the specific equation of state employed to describe matter at nuclear densities. These functions are normally referred to as “universal relations” and have been found to apply, within limits, both to static or stationary isolated stars, as well as to fully dynamical and merging binary systems. Further extending the idea that universal relations can be valid also away from stability, we show that a universal relation is exhibited also by equilibrium solutions that are not stable. In particular, the mass of rotating configurations on the turning-point line shows a universal behaviour when expressed in terms of the normalized Keplerian angular momentum. In turn, this allows us to compute the maximum mass allowed by uniform rotation, M_{\max} , simply in terms of the maximum mass of the nonrotating configuration, M_{TOV} , finding that $M_{\max} \simeq (1.203 \pm 0.022) M_{\text{TOV}}$ for all the equations of state we have considered. We further introduce an improvement to previously published universal relations by Lattimer & Schutz between the dimensionless moment of inertia and the stellar compactness, which could provide an accurate tool to constrain the equation of state of nuclear matter when measurements of the moment of inertia become available.

Key words: gravitational waves – binaries: general – stars: neutron.

1 INTRODUCTION

The behaviour of nuclear matter at the extreme densities reached in neutron-star cores is determined by the properties of fundamental interactions in regimes that are still poorly known and that are not accessible in experiments on Earth. A broad variety of different models for supernuclear matter, and thus for the inner structure of neutron stars, has been proposed. Although neutron-star properties depend sensitively on the equation of state (EOS), approximately “universal” relations between several dimensionless quantities have been found during the last years. The “universal” character in these relations comes from their weak dependence on the EOS and this allows one to use them to constrain quantities that are difficult to access experimentally, such as the neutron star radius.

Already in 1994, [Ravenhall & Pethick \(1994\)](#) highlighted an apparently universal relation between the normalized moment of inertia $I/(MR^2)$ and the stellar compactness M/R in the case of EOSs without an extreme softening at supernuclear densities. This relation was later refined by [Lattimer & Prakash \(2001\)](#) and [Bejger & Haensel \(2002\)](#), and then employed by [Lattimer & Schutz \(2005\)](#) to point out that using such an empirical relation it is possible to estimate the radius of a neutron star via the combined measurement of the mass and moment of inertia of a pulsar in a binary system. Additional evidence that EOS-independent relations could

be found among quantities characterizing compact stars was also pointed out by [Andersson & Kokkotas \(1998\)](#) [and later on revisited by [Benhar et al. \(2004\)](#)], who showed that a tight correlation exists between the frequency of the fundamental mode of oscillation and the stellar average density. More recently, however, [Yagi & Yunes \(2013b\)](#) have found that suitably normalized expressions for the moment of inertia I , the quadrupole moment Q and the tidal Love number λ are related by functions independent of the EOS to within $\sim 1\%$ in the slow-rotation approximation and assuming small tidal deformations [see also the related and earlier work by [Urbanec et al. \(2013\)](#); [Bauböck et al. \(2013\)](#)]. These relations are particularly useful as they may help remove some degeneracies as those appearing, for instance, in the modelling of the gravitational-wave signal from inspiralling binaries [see [Maselli et al. \(2013\)](#); [Yagi & Yunes \(2013a\)](#) for a discussion].

The universality, however, should be meant as approximate and is indeed preserved only within large but defined regimes, such as the slow-rotation approximation or when the magnetic fields are not particularly strong. More specifically, it has been shown by [Doneva et al. \(2014b\)](#) that the universality in the relation between I and Q breaks down in the case of rapid rotation for sequences with constant spin frequency. This result was partially revised by [Chakrabarti et al. \(2014\)](#), who have shown that the I –

Q universality is partly recovered if the rotation is characterized not by the spin frequency, but by the dimensionless angular momentum $j := J/M^2$, where J and M are the angular momentum and mass of the star, respectively [see also Pappas & Apostolatos (2014)]. At the same time, Haskell et al. (2014) have shown that the universality between I and Q is lost for stars with long spin periods, i.e., $P \gtrsim 10$ s, and strong magnetic fields, i.e., $B \gtrsim 10^{12}$ G. The reason behind this behaviour is rather simple: the anisotropic stresses introduced by a magnetic field can break the overall spherical symmetry present for stars that are nonrotating or in slow rotation. In turn, this affects the universal behaviour, which is based on the balance between gravity and the behaviour of fluids in strong gravitational fields.

Over the last couple of years, this area of research has been extremely active, with investigations that have considered universality also with higher multipoles (Chatziioannou et al. 2014; Yagi et al. 2014a; Pappas & Apostolatos 2014; Stein et al. 2014) or that have sought universality in response to alternative theories of gravity (Doneva et al. 2014a; Kleihaus et al. 2014; Pani & Berti 2014). A large bulk of work has also tried to provide a phenomenological justification for the existence of such a behaviour. For instance, it has been suggested that I , λ and Q are determined mostly by the behaviour of matter at comparatively low rest-mass densities, where realistic EOSs do not differ significantly because they are better constrained by nuclear-physics experiments (Yagi & Yunes 2013a). Alternatively, it has been suggested that the multipole moments approach the limiting values of a black hole towards high compactness, which implies that approximate no-hair-like relations exist also for non-vacuum spacetimes (Yagi et al. 2014b). Finally, it has been proposed that nuclear-physics EOSs are stiff enough that the nuclear matter can be modelled with an incompressible EOS. In this interpretation, low-mass stars, which are composed mainly of soft matter at low densities, would depend more sensitively on the underlying EOS, while the universality is much stronger towards higher compactness, where matter approaches the limit of an incompressible fluid (Martinon et al. 2014; Sham et al. 2015).

In this paper, we take a slightly different view and reconsider well-known universal relations to devise an effective tool to constrain the radius of a compact star from the combined knowledge of the mass and moment of inertia in a binary system containing a pulsar. More specifically, we first show that a universal relation holds for the maximum mass of uniformly rotating stars when expressed in terms of the dimensionless and normalized angular momentum. This relation extends and provides a natural explanation for the evidence brought about by Lasota et al. (1996) of a proportionality between the maximum mass allowed by uniform rotation and the maximum mass of the corresponding nonrotating configuration. Finally, we show that the dimensionless moment of inertia $\bar{I} := I/M^3$ for slowly rotating compact stars correlates tightly and universally with the compactness $\mathcal{C} := M/R$, where R is the radius of the star. Next, we provide an analytical expression for such a correlation and show that it improves on previous expressions, yielding relative errors in the estimate of the radius that are $\lesssim 7\%$ for a large range of masses and moment of inertia. We should note that universal relations \bar{I} – λ and λ – \mathcal{C} have been shown to hold by Yagi & Yunes (2013a) and Maselli et al. (2013), respectively. Hence, it is not surprising that a universal relation \bar{I} – \mathcal{C} also holds. However, to the best of our knowledge, this is the first time that such a relation is discussed in detail and that its implications are investigated in terms of astrophysical measurements.

The plan of the paper is as follows. In Section 2, we briefly review the mathematical and numerical setup used for the calculation

of our equilibrium stellar models (from nonrotating configurations to rapidly rotating ones). Section 3 is dedicated to our results and in particular to the new universal relation between the maximum mass and the normalized angular momentum. Section 4 is instead dedicated to the comparison between our expression for the dimensionless moment of inertia and previous results in the literature, while in Section 5 we discuss how the new relation can be used to deduce the radius of a compact star once a measurement is made of its mass and moment of inertia. Finally, Section 6 contains our conclusions and prospects for future work; the Appendix provides the derivation of an analytic expression to evaluate the relative error in the estimate.

2 MATHEMATICAL AND NUMERICAL SETUP

We have constructed a large number of equilibrium models of compact stars that are either nonrotating, slowly or rapidly rotating. In the first two cases, solutions can be obtained after the integration of ordinary differential equations in spherical symmetry, while in the third case we have made use of a two-dimensional numerical code solving elliptic partial differential equations.

More specifically, we consider the stellar matter as a perfect fluid with energy-momentum tensor (Rezzolla & Zanotti 2013)

$$T^{\mu\nu} = (e + p)u^\mu u^\nu + pg^{\mu\nu}, \quad (1)$$

where u^μ is the fluid 4-velocity, $g^{\mu\nu}$ the four-metric, while e and p are the fluid energy density and pressure, respectively. In the case of non-rotating stars, we take a spherically symmetric metric

$$ds^2 = -e^{2\phi(r)}dt^2 + e^{2\lambda(r)}dr^2 + r^2(d\theta^2 + \sin^2\theta d\varphi^2), \quad (2)$$

where $\phi(r)$ and $\lambda(r)$ are metric functions of the radial coordinate r only. Equilibrium models are then found as solutions of the Tolman–Oppenheimer–Volkoff (TOV) equations

$$\frac{dm(r)}{dr} = 4\pi r^2 e, \quad (3)$$

$$\frac{dp(r)}{dr} = \frac{(e + p)(m + 4\pi r^3 p)}{r(r - 2m)}, \quad (4)$$

$$\frac{d\phi(r)}{dr} = \frac{2}{(e + p)} \frac{dp}{dr}, \quad (5)$$

where the function $m(r)$ is defined as

$$m(r) := \frac{1}{2}r(1 - e^{-2\lambda}). \quad (6)$$

These TOV equations need to be supplemented with an EOS providing a relation between different thermodynamic quantities, and we have used 15 nuclear-physics EOSs in tabulated form. For all of them, beta equilibrium and zero temperature were assumed, so that the EOS reduces to a relation between the pressure and the rest-mass density (or the energy density). For more complex EOSs in which a temperature dependence is available, we have used the slice at the lowest temperature. In our analysis we have considered 28 several different theoretical approaches to the EOS and, in particular: the nuclear many-body theory [APR4, Akmal et al. (1998); WFF1, WFF2, Wiringa et al. (1988)], the non-relativistic Skyrme mean-field model [Rs, SK255, SK272, Ska, Skb, SkI2–SkI6, SkMp, Gulminelli & Raduta (2015), SLy2, SLy4, SLy9, Douchin & Haensel (2001); Gulminelli & Raduta (2015)], the mean-field theory approach [EOS L, Pandharipande & Smith (1975); HS DD2, HS NL3, HS TM1, HS TMA, SFHo, SFHx, Gaitanos et al. (2004); Hempel, M. and Schaffner-Bielich, J. (2010); Typel et al. (2010);

GShen-NL3, Shen et al. (2010), the Walecka model [EOS-O, Arnett & Bowers (1977)] and the liquid-drop model [LS220; Lattimer & Swesty (1991)]. All of these models are able to support a neutron star with a maximum mass of at least $2.0 M_{\odot}$ and are therefore compatible with the discovery of neutron stars with masses of about $2 M_{\odot}$ (Demorest et al. 2010; Antoniadis et al. 2013). At the same time, we note that because strong phase transitions above nuclear saturation density can affect the radii of low-mass neutron stars, determining whether a phase transition occurs (and if so at which rest-mass density) represents an important consideration not contemplated in these EOSs, but that will be the focus of future work.

It is possible to extend the validity of the TOV solutions by considering stellar models in the slow-rotation approximation (Hartle 1967)¹. In this case, spherical symmetry is still preserved, but rotational corrections do appear at first order in the stellar angular velocity Ω , and the line element (2) is replaced by its slow-rotation counterpart (Hartle 1967)

$$ds^2 = -e^{2\phi(r)} dt^2 + e^{2\lambda(r)} dr^2 + r^2 [d\theta^2 + \sin^2\theta (d\varphi - (\omega(r, \theta) + \mathcal{O}(\Omega^3)) dt)^2], \quad (7)$$

where $\phi(r)$, $\lambda(r)$ are still functions of the radial coordinate only and $\omega(r, \theta)$ represents the angular velocity of the inertial frames dragged by the stellar rotation. The set of equations (3)–(5) needs then to be augmented with a differential equation for the relative angular velocity

$$\frac{1}{r^4} \frac{d}{dr} \left(r^4 j \frac{d\bar{\omega}}{dr} \right) + \frac{4}{r} \frac{dj}{dr} \bar{\omega} = 0, \quad (8)$$

where $\bar{\omega} := \Omega - \omega(r)$ is the difference between the angular velocity ω acquired by an observer falling freely from infinity and the angular velocity of a fluid element measured by an observer at rest at some point in the fluid.

A numerical solution to equations (3)–(8) can be obtained by integrating them outwards from the stellar centre using, for instance, a fourth-order Runge-Kutta algorithm. At the stellar surface, $\bar{\omega}$ must be matched to the analytic exterior solution which has the form

$$\bar{\omega} = \Omega - \frac{2J}{r^3}, \quad (9)$$

where J is the total angular momentum of the star. The integration, which can be started with an arbitrary value for $\bar{\omega}$, can then be adjusted so as to match the boundary condition. Once a slowly rotating solution with angular momentum J and spin frequency Ω has been found, the corresponding moment of inertia can then be computed as

$$I := \frac{J}{\Omega} = \frac{R^4}{6\Omega} \left(\frac{d\bar{\omega}}{dr} \right)_R, \quad (10)$$

where the derivative in the last equality is meant to be taken at the stellar surface. Note that at this order the angular momentum J depends linearly on the angular velocity Ω , so that the moment of inertia does not depend on Ω . Quite generically, the moment of inertia increases almost linearly with the mass for sufficiently

small masses; however, as the maximum mass is approached, it decreases rapidly. This behaviour is due to the fact that I depends quadratically on the radius, which decreases significantly near the maximum mass.

We should note that treatments higher than the first-order in Ω have been also presented, in Hartle (1967, 1973), where even the third-order terms were included [see also Benhar et al. (2005)]. These treatments, however, are still not very accurate for rapidly rotating models of compact stars. Hence, we have relied on fully numerical solutions constructed using the open-source code RNS, which solves the Einstein equations in axisymmetry and in the conformally flat approximation (Stergioulas & Friedman 1995). In this case, the spacetime is assumed to be stationary and axisymmetric, and can be described by a metric of the form

$$ds^2 = -e^{\gamma+\epsilon} dt^2 + e^{2\alpha} (dr^2 + r^2 d\theta^2) + e^{\gamma-\epsilon} r^2 \sin^2\theta (d\varphi - \omega dt)^2, \quad (11)$$

where the metric potentials γ , ϵ , α and ω are functions of the quasi-isotropic coordinates r and θ . Stellar models can then be computed along sequences in which the central energy density and the axis ratio (or spin frequency) is varied (Stergioulas & Friedman 1995).

3 UNIVERSALITY AWAY FROM STABILITY

With the exception of those works that have looked at the existence of universality in merging systems of neutron-star binaries (Read et al. 2013; Maselli et al. 2013; Takami et al. 2014, 2015; Bernuzzi et al. 2014), all of the work done so far on universal relations in isolated relativistic stars has concentrated on *stable* equilibrium configurations. This is of course the most natural part of the space of parameters that is worth investigating. Yet, it is interesting to assess whether universality is present also for stellar models that are either marginally stable or that actually represent unstable equilibrium models. To this scope, we have investigated whether a universal behaviour can be found also for models whose gravitational mass is at the critical-mass limit or reasonably close to it.

We recall that Friedman et al. (1988) proved that a sequence of uniformly rotating barotropic stars is secularly unstable on one side of a turning point, i.e., when it is an extremum of mass along a sequence of constant angular momentum, or an extremum of angular momentum along a sequence of constant rest-mass. Furthermore, arguing that viscosity would lead to uniform rotation, they concluded that the turning point should identify the onset of secular instability. While for nonrotating stars the turning point does coincide with the secular-instability point (and with the dynamical-instability point for a barotropic star if the perturbation satisfies the same equation of state of the equilibrium model), for rotating stars it is only a sufficient condition for a secular instability, although it is commonly used to find a dynamical instability in simulations (Baiotti et al. 2005; Radice et al. 2010). More recently, Takami et al. (2011) have computed the neutral-stability line for a large class of stellar models, i.e., the set of stellar models whose F -mode frequency is vanishingly small; such a neutral-stability point in a nonrotating star marks the dynamical-stability limit. The latter coincides with the turning-point line of Friedman et al. (1988) for nonrotating stars, but differs from it as the angular momentum is increased, being located at smaller central rest-mass densities as the angular momentum is increased. Stated differently, the results of Takami et al. (2011) have shown that equilibrium stellar models on the turning-point line are effectively dynamically *unstable*. This result, which was also confirmed by numerical simulations, does

¹ The slow-rotation approximation normally refers to treatments that are truncated at first order in the spin frequency Ω . However, already in Hartle (1967), a full second-order treatment was developed, and subsequently applied by Hartle & Thorne (1968) for a systematic study of rotating relativistic stars.

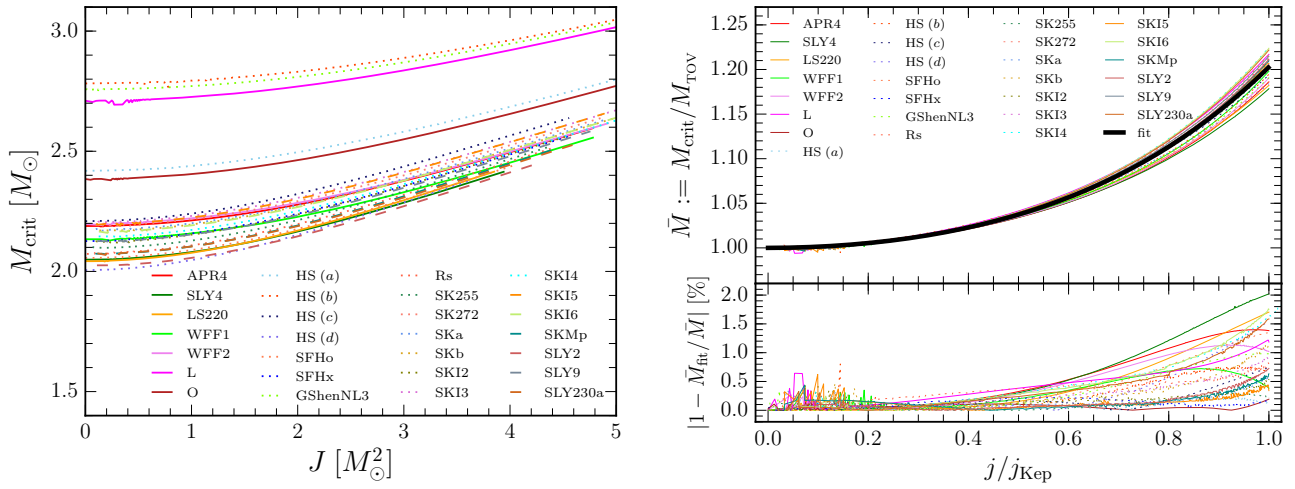


Figure 1. *Left panel:* “Critical” masses, i.e., masses of stellar models along the turning-point line, shown as a function of the corresponding angular momentum J and for a variety of EOSs. The EOSs HS (a)–HS (d) refer to HS DD2, HS NL3, HS TM1, and HS TMa, respectively. *Right panel:* The same data as in the left panel but when expressed in terms of dimensionless and normalised quantities: $M_{\text{crit}}/M_{\text{TOV}}$ and j/j_{Kep} . Shown with a black solid line is the polynomial fit (12), while the lower panel shows the relative deviation of the numerical data from the fitting function.

not contradict turning-point criterion since the latter is only a sufficient condition for secular instability [see also the discussion by [Schiffrin & Wald \(2014\)](#)].

Determining the critical mass in a way that is independent of the EOS is critical in many astrophysical scenarios, starting from those that want to associate Fast Radio Bursts ([Thornton et al. 2013](#)) to a “blitzar” and hence to the collapse of a supramassive neutron star ([Falcke & Rezzolla 2014](#)), over to those that apply this scenario to the merger of binary neutron-star systems ([Zhang 2014](#)) and are thus interested in the survival time of the merger to extract information on the EOS ([Lasky et al. 2014](#)), or to those scenarios in which the late collapse of the binary merger product can be used to explain the extended X-ray emission in short gamma-ray burst ([Zhang & Mészáros 2001](#); [Rezzolla & Kumar 2015](#); [Ciolfi & Siegel 2015](#)).

We should note that this is not the first time that “universal” relations in the critical mass are considered. Indeed, [Lasota et al. \(1996\)](#) have already discussed that there is a close correlation between the “mass-shedding” (or Keplerian) frequency Ω_{Kep} and the mass and radius of the maximum mass configuration in the limit of no rotation, i.e., M_{TOV} and R_{TOV} . Because larger masses can support larger Keplerian frequencies, the maximum critical mass is defined as the largest mass for stellar models on the critical (turning-point) line. After considering a large set of EOSs, [Lasota et al. \(1996\)](#) have shown that there exists a universal proportionality between the radii and masses of maximally rotating and of static configurations².

In view of the simplicity of computing stellar models on the turning-point line and given that these models are very close to those on the neutral-stability line, we have computed the maximum masses of models along constant angular momentum-sequences, i.e., such that $(\partial M / \partial \rho_c)_J = 0$, where ρ_c is the central rest-mass density. Although these models are strictly speaking unsta-

ble, for simplicity we have dubbed them “critical masses”, M_{crit} . The values of these masses as a function of the angular momentum J are reported in the left panel of Fig. 1, which shows that a large variance exists with the EOS when the data is reported in this way³. Each sequence terminates with the “maximum” (critical) mass that is supported via (uniform) rotation $M_{\text{max}} := M_{\text{crit}}(j = j_{\text{Kep}})$, where j_{Kep} is the maximum angular momentum that can be attained normalized to the maximum mass, i.e., $j_{\text{Kep}} := J_{\text{Kep}}/M_{\text{Kep}}^2$. Note that the maximum mass in this case can range from values as small as $M_{\text{max}} \simeq 2.2 M_{\odot}$ for $J \simeq 4 M_{\odot}^2$, up to $M_{\text{max}} \simeq 3.1 M_{\odot}$ for $J \simeq 5 M_{\odot}^2$.

The same data, however, can be expressed in terms of dimensionless quantities and, more specifically, in terms of the critical mass normalized to the maximum value of the corresponding non-rotating configuration, i.e., $\bar{M} := M_{\text{crit}}/M_{\text{TOV}}$ and of the dimensionless angular momentum j when the latter is normalized to the maximum value allowed for that EOS, j_{Kep} . Such a data is collected in the right panel of Fig. 1 and shows that the variance in this case is extremely small. Indeed, it is possible to express such a behaviour with a simple polynomial fitting function of the type

$$\frac{M_{\text{crit}}}{M_{\text{TOV}}} = 1 + a_2 \left(\frac{j}{j_{\text{Kep}}} \right)^2 + a_4 \left(\frac{j}{j_{\text{Kep}}} \right)^4, \quad (12)$$

where the coefficients are found to be $a_2 = 1.316 \times 10^{-1}$ and $a_4 = 7.111 \times 10^{-2}$, with a reduced chi squared $\chi_{\text{red}}^2 = 3.586 \times 10^{-5}$ and where, of course, $M_{\text{crit}} = M_{\text{TOV}}$ for $j = 0$.

An immediate consequence of Eq. (12) is also a very important result. Irrespective of the EOS, in fact, the maximum mass that can be supported through uniform rotation is simply obtained after

² Interestingly, the concept of universality is already pointed out clearly in [Lasota et al. \(1996\)](#), although it refers to a single value of the universal relation (i.e., the maximum mass) and not to the whole functional behaviour.

³ The data for large masses and small values of the angular momentum is somewhat noisy, as this represents a difficult limit for the RNS code ([Stergioulas & Friedman 1995](#)); we could have used the slow-rotation approximation to compute the data in this limit, but we have preferred to perform the analysis on a single dataset.

setting $j = j_{\text{Kep}}$ and is therefore given by

$$M_{\text{max}} := M_{\text{crit}}(j = j_{\text{Kep}}) = (1 + a_2 + a_4) M_{\text{TOV}} \simeq (1.203 \pm 0.022) M_{\text{TOV}}, \quad (13)$$

where we have taken as error not the statistical one (which would be far smaller) but the largest one shown in the comparison between the fit and the data.

In summary, although different EOSs give substantially different maximum masses and are able to reach substantially different angular momenta, the maximum mass that can be supported at the mass-shedding limit is essentially universal and is about 20% larger than the corresponding amount in the absence of rotation. Also shown in the bottom part of the panel is the relative error between the normalised critical mass \bar{M} and its estimate coming from the fit (12), M_{fit} . Note that the error for the largest angular momentum is below 2% for all the EOSs considered and that it is below 1% for most rotation rates.

Similar conclusions on the maximum mass were reached also by Lasota et al. (1996), although with a larger variance, probably due to the use of EOSs that did not satisfy the constraint of $M_{\text{TOV}} > 2 M_{\odot}$ and different normalizations. This confirms the idea that the uncertainties in correlations of this type could be further reduced if future observations will increase the value of the maximum mass M_{TOV} (Lattimer 2015). More importantly, expression (12) highlights that a universal relation is present not only for the maximum critical mass, but is valid also for any value of the dimensionless angular momentum, with a variance that is actually smaller for slowly rotating models. This is a result that was not discussed by Lasota et al. (1996).

Despite the important implications that expression (12) has, its use in the form above is very limited as it requires the implicit knowledge of M_{crit} , as well as of j and j_{Kep} . A way around this limitation is possible if one makes the reasonable assumption that for a given angular momentum, the mass and radius of the mass-shedding model is proportional to the mass and radius of the maximum-mass nonrotating model, i.e.,

$$M_{\text{Kep}} \simeq b_1 M_{\text{TOV}}, \quad R_{\text{Kep}} \simeq b_2 R_{\text{TOV}}, \quad (14)$$

and that the Keplerian frequency follows the classical scaling in mass and radius

$$\Omega_{\text{Kep}} \simeq \sqrt{M_{\text{Kep}}/R_{\text{Kep}}^3} \simeq b_3 \sqrt{M_{\text{TOV}}/R_{\text{TOV}}^3}. \quad (15)$$

As a result, the angular momentum at the mass-shedding limit can be expressed also as a function of the maximum-mass nonrotating configuration

$$J_{\text{Kep}} = I_{\text{Kep}} \Omega_{\text{Kep}} \simeq M_{\text{Kep}} R_{\text{Kep}}^2 \Omega_{\text{Kep}} \simeq b_4 \sqrt{M_{\text{TOV}}^3 R_{\text{TOV}}}, \quad (16)$$

and thus

$$j_{\text{Kep}} = J_{\text{Kep}}/M_{\text{Kep}}^2 \simeq b_4 \sqrt{R_{\text{TOV}}/M_{\text{TOV}}} = b_4 \sqrt{1/\mathcal{C}_{\text{TOV}}}. \quad (17)$$

The coefficients b_1 , b_2 , and b_3 can be computed via a fit to the data, yielding: $b_1 = 1.204 \pm 0.002$, $b_2 = 1.310 \pm 0.014$, and $b_3 = (6.303 \pm 0.022) \times 10^{-1}$, while the coefficient b_4 can be derived as $b_4 = b_1 b_2^2 b_3$. Alternatively, and more accurately, b_4 can be computed via a direct fit of expression (16), which then yields $b_4 = (5.543 \pm 0.068) \times 10^{-1}$.

We can now use expression (17) in the dimensionless fit (12) to obtain

$$M_{\text{crit}} = (1 + c_2 \mathcal{C}_{\text{TOV}} j^2 + c_4 \mathcal{C}_{\text{TOV}}^2 j^4) M_{\text{TOV}}, \quad (18)$$

where the coefficients have numerical values $c_2 = 4.283 \times 10^{-1}$ and $c_4 = 7.533 \times 10^{-1}$. Expression has the desired features, since the critical mass is now function only of the stellar angular momentum J and of the properties (mass and radius) of the maximum-mass nonrotating configuration, M_{TOV} and R_{TOV} . Note that expression (18) is not in an explicit form, since the right-hand side still contains information on the critical mass via $j = J/M_{\text{crit}}^2$. However, a simple root-finding algorithm can be used to obtain M_{crit} once J , M_{TOV} , and R_{TOV} are specified.

4 I- \mathcal{C} UNIVERSAL RELATIONS

In what follows we discuss universal relations between the moment of inertia I and the compactness \mathcal{C} . We will first consider the case of slowly rotating stars (Section 4.1) and then that of rapidly rotating ones (Section 4.2).

4.1 I- \mathcal{C} relations for slowly rotating stars

Starting with Ravenhall & Pethick (1994), a number of authors have pointed out that the dimensionless moment of inertia $\tilde{I} := I/(MR^2)$ can be expressed in terms of the stellar compactness \mathcal{C} via simple low-order polynomial expressions that have a weak dependence on the EOS. Expressions of this type have been proposed by Lattimer & Prakash (2001), as well as by Bejger & Haensel (2002), with comparable level of precision. A higher-order polynomial fit was proposed subsequently by Lattimer & Schutz (2005) (LS), who expressed it as

$$\tilde{I} := \frac{I}{MR^2} = \tilde{a}_0 + \tilde{a}_1 \mathcal{C} + \tilde{a}_4 \mathcal{C}^4, \quad (19)$$

and discussed how such a relation could be used to constrain the stellar radius once I and M are measured, e.g., in a pulsar within a binary system.

The left panel of Fig. 2 reports with a scatter plot the values of \tilde{I} relative to slowly rotating stars [i.e., stars treated in the slow-rotation approximation (7)] as computed for a number of different EOSs and in a large range of compactnesses, i.e., with $\mathcal{C} \in [0.07, 0.32]$; this is also the range in compactness over which the fits are performed. Different symbols and colours refer to different EOSs as reported in the legend. Also indicated with a black solid line is the LS fit expressed by (19), while the shaded band reports the error in the fitting coefficients.

The fitting coefficients found originally by Lattimer & Schutz (2005) are: $\tilde{a}_0 = 0.237 \pm 0.008$, $\tilde{a}_1 = 0.674$ and $\tilde{a}_4 = 4.48$, while those produced by our analysis are slightly different and given by: $\tilde{a}_0 = 0.244$, $\tilde{a}_1 = 0.638$ and $\tilde{a}_4 = 3.202$. The main differences in the estimates (especially in the quartic term) are due to the different set of EOSs used and, more importantly, to the fact that the estimates by Lattimer & Schutz (2005) were based in part on EOSs which are now excluded by observations of a 2 M_{bigodot} neutron star.

Lattimer & Prakash (2001) and Lattimer & Schutz (2005) found that fitting functions of the type (19) were valid for a wide range of EOS except the ones which exhibited extreme softening. This is measured by the relative error $|1 - \tilde{I}/\tilde{I}_{\text{fit}}|$, which is reported in the lower part of the left panel of Fig. 2, and which shows the errors are generally below 10%. At the same time, the large scatter of the data suggests that a tighter fit could be obtained if a different normalization is found for the moment of inertia. Hence, inspired by the normalization's proposed by Lau et al. (2010) and

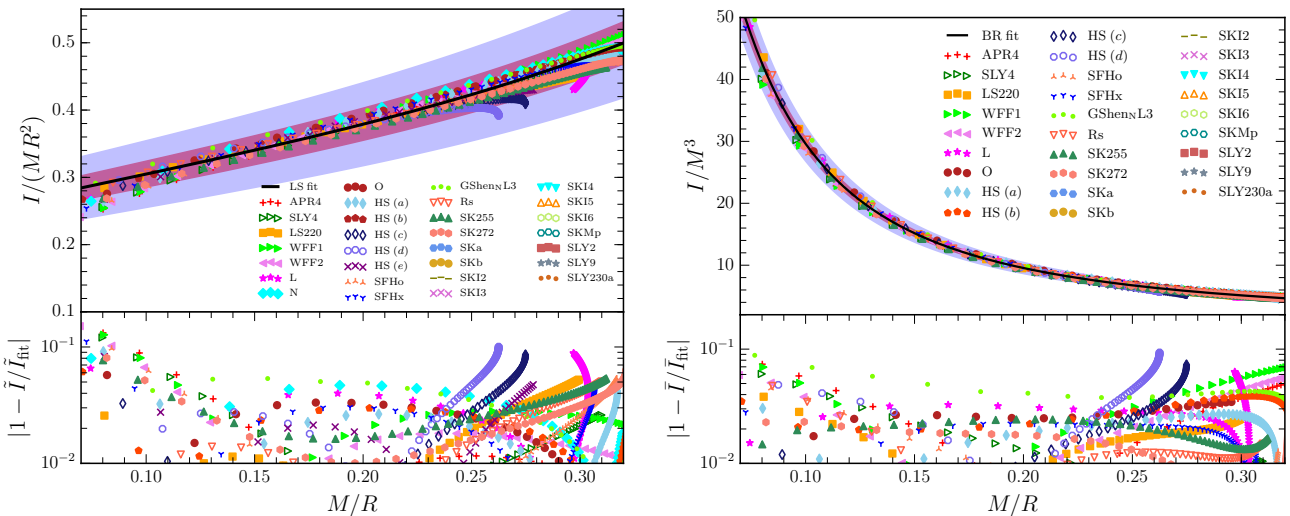


Figure 2. *Left panel:* Normalized moment of inertia $I/(MR^2)$ shown as a function of the stellar compactness \mathcal{C} , and for different EOSs, each indicated with a different symbol. The solid black line reports the fitting function (19) suggested by Lattimer & Schutz (2005). *Right panel:* Normalized moment of inertia I/M^3 shown as a function of stellar compactness \mathcal{C} ; also in this case, the solid black line reports the fitting function Eq. (20). In both panels the red- and blue-shaded areas refer respectively to the values of $\langle L_\infty \rangle$ and L_∞ , where $\langle L_\infty \rangle$ is the average over all EOSs of the largest residual $|1 - \bar{I}/\bar{I}_{\text{fit}}|$, while L_∞ is the largest residual across all EOSs (cf., Table 1). Note that only 10% of the points used in the analysis is shown in the plots.

	$\langle L_1 \rangle$	$\langle L_2 \rangle$	$\langle L_\infty \rangle$	L_∞
$I/(MR^2)$	0.01711	0.00080	0.06294	0.16268
I/M^3	0.01068	0.00043	0.03209	0.09420

Table 1. Summary of various averaged norms of the residuals of the two fits, i.e., the averages over all EOSs of all the residuals $|1 - \bar{I}/\bar{I}_{\text{fit}}|$ when normalizing the moment of inertia as $I/(MR^2)$ or I/M^3 , respectively. The last column reports instead the largest infinity norm, i.e., the largest residual across all EOSs. The values of the last two columns are reported as shaded areas (red and blue, respectively) in Fig. 2.

Yagi & Yunes (2013a), we have considered to fit the moment of inertia through a functional expansion of the type

$$\bar{I} := \frac{I}{M^3} = \bar{a}_1 \mathcal{C}^{-1} + \bar{a}_2 \mathcal{C}^{-2} + \bar{a}_3 \mathcal{C}^{-3} + \bar{a}_4 \mathcal{C}^{-4}. \quad (20)$$

There are two main motivations behind this choice. The first one is that it is clear that at lowest order $I/M^3 \sim 1/\mathcal{C}^2$ and hence an expansion in terms of inverse powers of the compactness is rather natural. The second one is the realisation that universal relations exist between I/M^3 and λ (Yagi & Yunes 2013b) and between λ and \mathcal{C} (Maselli et al. 2013), so that a universal relation should also exist also between I/M^3 and \mathcal{C} , although not yet discussed in the literature.

The right panel of Fig. 2 shows the same data as in the left panel but with the new normalisation I/M^3 and the new fitting function (20) with a black solid line, while the shaded grey band reports the error in the fitting coefficients. The behaviour of the moment of inertia is now on average more accurately captured, with a behaviour which is essentially universal and relative errors which are comparable but also smaller than those of the fit (19)⁴. More precisely, the $\langle L_1 \rangle$ norm of the residuals of

the two fits, i.e., the average over all EOSs of all the residuals $|1 - \bar{I}/\bar{I}_{\text{fit}}|$) is given by $\langle L_1 \rangle \simeq 1.7\%$ for the fit of $I/(MR^2)$ and by $\langle L_1 \rangle \simeq 1.1\%$ for the fit of I/M^3 . Similar are also the values of the $\langle L_\infty \rangle$ norms (i.e., the largest relative deviation between the data and the fits), which are 6% and 3%, respectively. A summary of the values of the various norms is shown in Table 1, where the values of the last two columns are reported as shaded areas (red and blue, respectively) in Fig. 2. Not surprisingly, the largest errors are seen for very stiff (small \mathcal{C}) or very soft (large \mathcal{C}) EOSs. The numerical values of the fitting coefficients in Eq. (20) are summarised in Table 2, together with the corresponding reduced chi squared.

Three remarks are worth making. First, the fitting (20) could be further improved if the normalization of the moment of inertia is modified in terms of dimensionless quantities, e.g., a given power of the compactness as suggested by Majumder et al. (2015). While useful to tighten the fit, we are not certain that this approach is effective in general or provides additional insight; hence, we will not adopt it here. Second, the quantity \bar{I} is sometimes associated to what is called the “effective compactness” $\eta := \sqrt{M^3/\bar{I}} \sim M/R$ (Lau et al. 2010), where one is considering that $I \sim MR^2$. Clearly, as the fit in expression (20) reveals, this association is reasonable only at the lowest order. Finally, while the relation \bar{I} - \mathcal{C} provides a description of the universal behaviour of the moment of inertia that is slightly more accurate than the one captured by the \tilde{I} - \mathcal{C} relation, the visual impression provided by Fig. 2 enhances the impression of a better fit for the \bar{I} - \mathcal{C} relation. In practice, the much larger range span by \bar{I} across the relevant compactnesses induces one to believe that the universality is far superior in this latter case. As testified by the data in the lower plots, the error is, on average, only slightly smaller.

magnitudes, the use of a χ^2 would not be sensible for a comparison of the goodness of the fits.

⁴ We note that since $I/(MR^2)$ and I/M^3 have intrinsically different

	\bar{a}_1	\bar{a}_2	\bar{a}_3	\bar{a}_4	χ^2_{red}
slow rot.	8.134×10^{-1}	2.101×10^{-1}	3.175×10^{-3}	-2.717×10^{-4}	1.184×10^{-1}
$j = 0.2$	9.426×10^{-1}	1.541×10^{-1}	1.117×10^{-2}	-7.004×10^{-4}	8.579×10^{-2}
$j = 0.4$	9.499×10^{-1}	1.436×10^{-1}	1.220×10^{-2}	-7.613×10^{-4}	1.047×10^{-1}
$j = 0.6$	7.408×10^{-1}	2.288×10^{-2}	-2.975×10^{-3}	-9.895×10^{-5}	1.655×10^{-1}

Table 2. Summary of the fitting coefficients for the universal \bar{I} - \mathcal{C} relation (20) as obtained in the slow-rotation approximation or along sequences of constant dimensionless spin parameter. Also shown in the last column is the corresponding reduced chi squared.

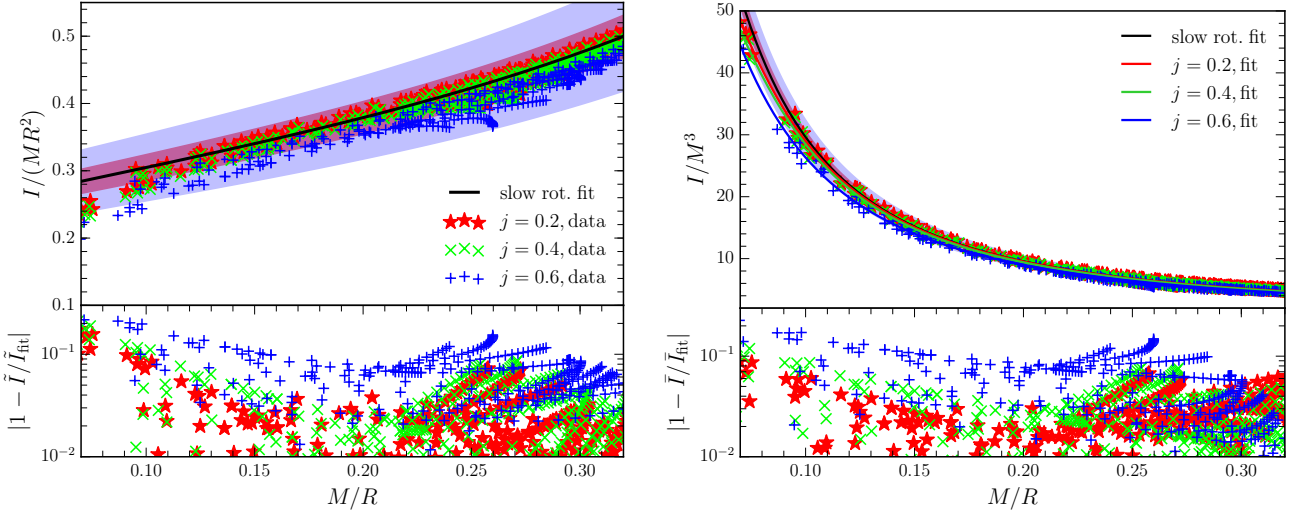


Figure 3. Left panel: Normalized moment of inertia $I/(MR^2)$ shown as a function of the stellar compactness \mathcal{C} . Different symbols refer to different EOSs, while symbols of a given colour refer to a certain value of the normalized angular momentum: $j = 0.2$ (red symbols), $j = 0.4$ (green symbols), and $j = 0.6$ (blue symbols). The shaded area marks the uncertainty band of the fitting function for I in the slow-rotation approximation, while the bottom panel shows the relative error with respect to the fit (also in this case only 10% of the points used in the analysis is shown in the plots). Right panel: The same as in the left panel but for the normalized moment of inertia I/M^3 . In both panels, the light shaded areas refer to the values of the L_∞ norms of the residuals for the slowly rotating stellar models, while the dark shaded areas mark the average of the L_∞ norms over all EOSs. Overall, the data show that the universal behaviour found in the slow-rotation approximation is valid, within the errors, also for rapidly rotating stars.

4.2 I - \mathcal{C} relations for rapidly rotating stars

As mentioned in Section 2, within the slow-rotation approximation the properties of the compact stars do not depend on the magnitude of rotation and the surface is still given by a 2-sphere of constant radial coordinate. When the stars are rapidly rotating, on the other hand, not only the effect of the frame dragging needs to be included, but also the change in the stellar surface needs to be taken into account. More specifically, as a rotating star approaches the “mass-shedding” (or Keplerian) limit, that is, the limit at which it is spinning so fast so as to lose matter at the equator, its mass and equatorial radius increase while the polar radius decreases, leading to an overall oblate shape. Since the moment of inertia is influenced mostly by the mass in the outer regions of the star, the increases in mass and radius lead quite generically to larger moments of inertia.

Since the I - λ - Q universal relations were first discussed in the limit of slow rotation and small tidal deformations, Doneva et al. (2014b) have investigated the impact of rapid uniform rotation on these relations and, in particular, on the between the moment of inertia for sequences with constant angular velocity Ω . What was found in this case is that the \bar{I} - Q universality was lost, with deviations from the slow-rotation limit of up to 40% with increasing rotation rate. Interestingly, however, Chakrabarti et al. (2014) also

found that the universality is restored (within limits) if the dimensionless moment of inertia is ordered not along sequences of constant Ω , but along sequences of constant dimensionless spin parameter $j := J/M^2$. In particular, along each sequence the \bar{I} - Q relation is independent of the EOS up to about 1%, but it is of course a function of the spin parameter j .

Hence, it is natural to investigate whether the \bar{I} - \mathcal{C} relation we have discussed in the previous Section in the case of slowly rotating stars, continues to be valid also in the case of rapid rotation. This is summarised in Fig. 3, whose two panels show respectively \bar{I} and \bar{I} as a function of \mathcal{C} , with the shaded band marking the uncertainty band coming from the fit within the slow-rotation approximation⁵. Following Chakrabarti et al. (2014), and expecting it will yield a tighter correlation, we order the data along sequences of constant j . Note that while the data for $j = 0.2$ (red symbols) lies almost on top of the results for the slow-rotation limit, the sequences for $j = 0.4$ (light-green) show larger deviations, and for $j = 0.6$ (blue symbols) the data lies completely outside of the error band for the

⁵ To avoid overloading the figure, which has now four times the amount of data shown in Fig. 2, the data reported in Fig. 3 refers only to the first EOSs in Fig. 2, i.e., EOSs: APR4, Sly4, LS220, WFF1, WFF2, L, N, O, HS (a), HS (b), HS (c), HS (d), SFHo, SFHx.

slow-rotation fit. Indeed, along the $j = 0.6$ sequence, which is also near the mass-shedding limit for most EOSs, the deviation in the fitted range can be as large as 20%.

Despite the complete loss of universality at high rotation rates and small compactnesses, and the fact that universality is present only along specific directions (i.e., $j = \text{const.}$ sequences), the \tilde{I} – \mathcal{C} relation remains effective for a large portion of the space of parameters. We recall, in fact, that the fastest known rotating pulsar has a spin frequency of 716 Hz (or a period of $\simeq 1.4$ ms, [Hessels et al. 2006](#)), which could correspond to $j \lesssim 0.5$ depending on the pulsar’s mass ([Stein et al. 2014](#)). For the EOSs used here, however, $j \lesssim 0.3$ for this pulsar and would therefore lie within the error band of the fit for the slow-rotation limit for most of that range. For completeness, and following what was done for the slow-rotation approximation, we report in Table 2 the numerical values of the fitting coefficients in Eq. (20) for the various $j = \text{const.}$ sequences considered.

4.3 Universal relations with the binding energy

Already [Lattimer & Prakash \(2001\)](#) had pointed out that the binding energy of a compact star, defined as the difference between the total rest mass M_b and the gravitational mass of an equilibrium configuration, $\text{BE} := M_b - M$ could show a behaviour that is essentially independent of the EOS. In particular, considering the dimensionless binding energy BE/M , [Lattimer & Prakash \(2001\)](#) found a good fit to the data with an expression of the type

$$\frac{\text{BE}}{M} = \frac{c_1 \mathcal{C}}{1 - c_2 \mathcal{C}}, \quad (21)$$

where $c_1 = 0.6$ and $c_2 = 0.5$. We have revisited the ansatz (21) using more modern EOSs satisfying the two solar-mass constraint and found that the fit to the data yields values for the coefficients and in particular that $c_1 = 6.213 \times 10^{-1}$ and $c_2 = 1.941 \times 10^{-1}$. The reduced chi squared for the two different sets of coefficients is different, being $\chi_{\text{red}}^2 = 8.254 \times 10^{-4}$ for the original fit of [Lattimer & Prakash \(2001\)](#) and of $\chi_{\text{red}}^2 = 7.553 \times 10^{-5}$ for our new fit.

Yet, because expression (23) is effectively a second-order polynomial for small values of \mathcal{C} , we have also considered a different functional form for the fitting ansatz and which, in the spirit of expression (20), is a quadratic polynomial in the stellar compactness, i.e.,

$$\frac{\text{BE}}{M} = d_1 \mathcal{C} + d_2 \mathcal{C}^2, \quad (22)$$

where $d_1 = 6.19 \times 10^{-1}$ and $d_2 = 1.359 \times 10^{-1}$. The fit in this case is marginally better than that obtained with expression (22), with a reduced chi square of $\chi_{\text{red}}^2 = 7.547 \times 10^{-5}$. All things considered, and on the basis of the EOSs used here, expression (22) is only a marginally better description of the functional behaviour of the reduced binding energy and should be considered effectively equivalent to expression (21).

Interestingly, expression (22) can also be easily extended to encompass the case of rotating stars after replacing the coefficients d_1 and d_2 with new expressions that contain rotation-induced corrections in terms of the dimensionless angular momentum, i.e., $d_1 \rightarrow \tilde{d}_1$ and $d_2 \rightarrow \tilde{d}_2$ in (22), where

$$\tilde{d}_1 := d_1(1 + \alpha j + \beta j^2), \quad \tilde{d}_2 := d_2(1 + \gamma j + \delta j^2), \quad (23)$$

where $\alpha = -1.966 \times 10^{-2}$, $\beta = 4.272 \times 10^{-1}$, $\delta = -7.603$, and $\gamma = 4.46 \times 10^{-1}$. Note that the linear coefficients are very small, as are the errors in the estimates of the quadratic coefficients.

The reduced chi square obtained when comparing the values of the reduced binding energy BE/M obtained via (22)–(23) with those obtained from the RNS is rather small and given by $\chi_{\text{red}}^2 = 1.624 \times 10^{-4}$. Finally, we note that expressing the binding energy in terms of the radius rather than of the mass changes the functional behaviour of the fitting function since $\text{BE}/R \sim \mathcal{C}^2$, but not the overall quality of the fit.

5 APPLICATIONS OF THE UNIVERSAL RELATION

While the origin of the universal relations is still unclear and the subject of an intense research (and debate), we take here the more pragmatic view in which universal relations are seen as an interesting behaviour of compact stars in a special area of the space of solutions: namely, those of slowly rotating, low-magnetisation stars. In this view, universal relations can be used to constrain phenomenologically quantities which are not directly accessible by observations or whose behaviour is degenerate. For instance, the simultaneous measurement of the mass and of the moment of inertia of a compact star, e.g., of a pulsar in a binary system of compact stars, does not necessarily provide information on the radius. On the other hand, the same measurements, together with the use of the universal relation (20) can set constraints on the radius and hence on the EOS. To illustrate how this can be done in practice let us consider the case in which the moment of inertia is measured with an observational error of 10%; this may well be an optimistic expectation but is not totally unrealistic [a similar assumption was made also by [Lattimer & Schutz \(2005\)](#)]. If the mass is observed with a much larger precision [as it is natural to expect from pulsar measurements in binary neutron-star systems ([Kramer & Wex 2009](#))], then it is possible to define regions in the (M, R) plane that are compatible with such observations. In turn, the comparison with the expectations from different EOSs will set constraints on the radius of the star.

In practice, given a measurements of I and M , it is sufficient to invert the fitting function (20) to obtain the range of radii that is compatible with the measurements of I and M . Examples of these compatibility regions in the (M, R) plane are represented by the coloured shaded regions in the left panel of Fig. 4, where we have considered respectively $I = 50 M_\odot \text{ km}^2$ (red-shaded region), $I = 80 M_\odot \text{ km}^2$ (green-shaded region), and $I = 120 M_\odot \text{ km}^2$ (blue-shaded region)⁶. Given then a measure of the mass (we have considered a canonical mass of $M = 1.4 M_\odot$ and indicated it with an horizontal black dashed line), the intersection of the corresponding constraint with a given shaded region sets a range for the possible value of the radius. For instance, a measurement of $I = 80 M_\odot \text{ km}^2$ and $M = 1.4 M_\odot$ would require radii in excess of $\simeq 12$ km, thus excluding relatively soft EOSs such as APR4.

Similar considerations can be made also for rapidly rotating stars. This is shown as is shown in the right-hand panel of Fig. 4, where we consider again three different hypothetical measurements of the moment of inertia, but also consider the extension of the universal relation (20) along sequences of constant dimensionless spin parameter j . We indicate with a black solid line the fit relative to the slowly rotating models and with red, green and blue dashed lines the fits corresponding to $j = 0.2$, 0.4 , and $j = 0.6$, respectively. Note that even the largest considered value for j , the sequences are

⁶ Note that the shaded bands include both an observational error on the moment of inertia of 10% and the error on the fit coming from Eq. (20).

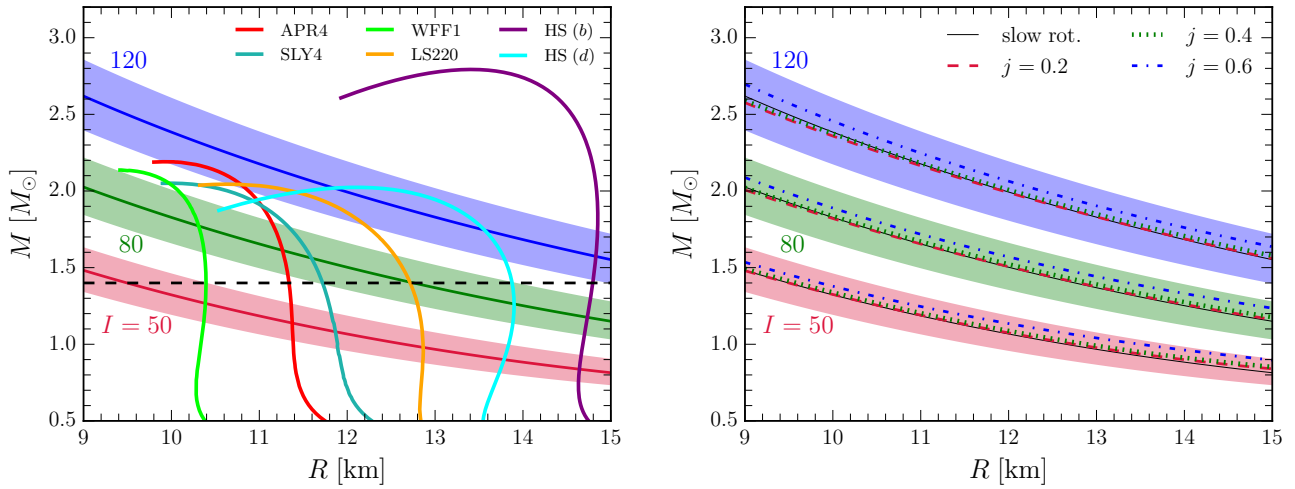


Figure 4. *Left panel:* Solid lines of different colours indicate the mass-radius relations for nonrotating stellar models for some representative EOSs. The red, green, and blue solid lines indicate instead the mass-radius relations as constrained by a measurement of the moment of inertia and through the inversion of Eq. (20). In particular, the red, green, and blue lines refer to moments of inertia of $I = 50, 80$ and $120 M_{\odot} \text{ km}^2$, respectively. The corresponding shaded bands include an observational error on the moment of inertia of 10% and the uncertainty in the fitting coefficients. The black dashed line shows the specific case of a mass measurement of $M = 1.4 M_{\odot}$. *Right panel:* The same as in the left panel, but for rotating models organised in sequences of constant spin parameter j (red, green, and blue dashed lines for $j = 0.2, 0.4$ and $j = 0.6$, respectively). Note that the curves for the rotating models lie within the error bands of the mass-radius relations computed for slowly rotating stars.

within the error bands imposed by the observational error on I and by the uncertainties on the fitting function.

Following the considerations above, we next compute the error made in estimating the radius of the star for any EOS once a measurement is made of I and M . To this scope we need to account both for the error due to the observational uncertainty of the moment of inertia and for the error on the fitting function. Because the error on the fit (20) is of the order of 5% for a large part of the considered range in the compactness, the error on the radius made when inverting the fitting function (20) can be estimated via the standard Gaussian error-propagation law. More specifically, we assume that the total error in the radius estimate is given by the sum in quadrature of two errors, i.e.,

$$\sigma_R = \sqrt{\sigma_{\text{fit}}^2 + \sigma_{I_{\text{obs}}}^2}, \quad (24)$$

where σ_{fit} is the error in the fit when computed as the L_{∞} -norm of the relative deviation of the fit from the data [cf., Eq. (25)], while $\sigma_{I_{\text{obs}}}$ is the error in the observed moment of inertia. The error on the fit is approximately given by

$$\sigma_{\text{fit}}^2 = \bar{I}^2 L_{\infty}^2, \quad (25)$$

where L_{∞} is the maximum relative error $(1 - \bar{I})/\bar{I}$. Of course, all what was discussed so far can be applied equally to the new fitting relation (20) as to the original fit by Lattimer & Schutz (2005) given by expression (19).

Figure 5 summarises the results of this error analysis by reporting the relative error in the measurement of the stellar radius $\Delta R/R$ for any EOS once the mass of the star is measured to high precision and the moment of inertia is estimated with a relative error of 10%. More specifically, Eqs. (19) and (20) are inverted numerically to estimate R from M and I , while ΔR is computed as the difference between the radius obtained from the inverted fitting function and the inverted relation with the errors on the moment of inertia and the fitting function taken into account.

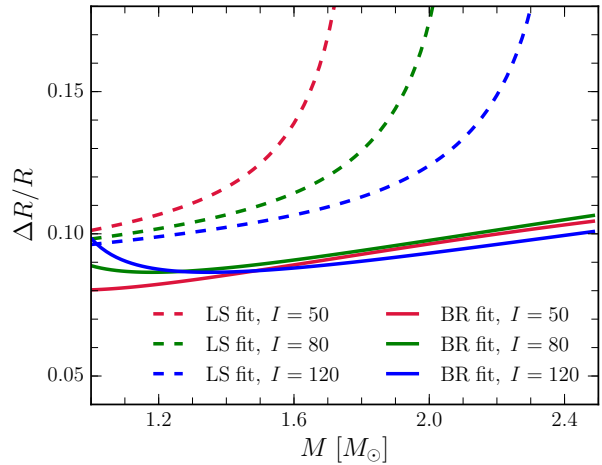


Figure 5. Relative error on the radius obtained either from the fit (19) (LS fit, dashed lines), or from the fit (20) (BR fit, solid lines). Different colours refer to different values of the moment of inertia (red, green and blue lines for $I = 50, 80$ and $120 M_{\odot} \text{ km}^2$, respectively). The error estimates include an observational uncertainty of the moment of inertia of 10% and the error on the fitting function.

Figure 5 shows this relative error $\Delta R/R$ as a function of the measured mass and also in this case we report with lines of different colours the three different hypothetical measurements of the moment of inertia. Note that we indicate with solid lines the errors deduced using the new fit (20) (BR fit) and with dashed lines the corresponding fit coming from expression (19) of Lattimer & Schutz (2005) (LS fit).

The two prescriptions provide rather different behaviours in the error estimates as a function of mass. In particular, for small

masses, i.e., $M \lesssim 1.4 M_{\odot}$, the modelling in terms of \tilde{I} and \tilde{I} yield comparable errors. However, for large masses, i.e., $M \gtrsim 1.4 M_{\odot}$, the modelling in terms of \tilde{I} yields considerably smaller errors.

6 CONCLUSIONS

We have shown that a universal relation is exhibited also by equilibrium solutions that are not stable. In particular, we have considered uniformly rotating configurations on the turning-point line, that is, whose mass is an extremum along a sequence of constant angular momentum. Such stellar configurations are unstable since they are found at larger central rest-mass densities than those that on the neutral-point line and therefore marginally stable (Takami et al. 2011). While hints of this relation were already discussed in the literature (Lasota et al. 1996), we have here shown that it holds not only for the maximum value of the angular momentum, but also for any rotation rate. The importance of this universal relation is that it has allowed us to compute the maximum mass sustainable through rapid uniform rotation, finding that for any EOS it is about 20% larger than the maximum mass supported by the corresponding nonrotating configuration.

Finally, using universal relations for some of the properties of compact stars, we have revisited the possibility of constraining the radius of a compact star from the combined measurement of its mass and moment of inertia, as is expected to be possible in a binary system containing a pulsar. In particular, after considering both stellar models in the slow-rotation approximation and in very rapid rotation, we have shown that the dimensionless moment of inertia $\tilde{I} = I/M^3$ for slowly rotating compact stars correlates tightly and universally with the stellar compactness $\mathcal{C} = M/R$ in a manner that does not depend on the EOS. We have also derived an analytical expression for such a correlation, which improves on a previous expression obtained with the dimensionless moment of inertia $\tilde{I} = I/(MR^2)$ (Lattimer & Schutz 2005).

Assuming that a measurement of the moment of inertia is made with a realistic precision of 10% and that a much more accurate measurement is made of the mass, we have found that the new relation yields relative errors in the estimate of the stellar radius that are $\lesssim 7\%$ for a large range of masses and moment of inertia. Radius measurements of this precision have the potential of setting serious constraints on the EOS. Interestingly, the universal relation between \tilde{I} and \mathcal{C} is not restricted to slowly rotating models, but can be found also in stellar models that are spinning near the mass-shedding limit. In this case, the universal relation needs to be parameterized in terms of the dimensionless angular momentum, but the functional behaviour is very close to the nonrotating limit also at the most extreme rotation rates.

7 ACKNOWLEDGEMENTS

We thank V. Ferrari, B. Haskell, and J. Lattimer for useful discussions and comments. We are also grateful to J. C. Miller for a careful read of the paper, to S. Typel for essential help with the use of CompOSE, and to the referee for useful comments and suggestions. LR thanks the Department of Physics of the University of Oxford, where part of this work was carried out. Partial support comes also from “NewCompStar”, COST Action MP1304, and by the LOEWE-Program in HIC for FAIR. All of the EOSs used here can be found at the EOS repository “CompStar On-

line Supernovae Equations of State (CompOSE)”, at the URL compose.obspm.fr.

8 NOTE ADDED IN PROOF

Since the posting of this paper, a number of related works have been published or posted. Bhattacharyya et al. (2016) have considered rapidly rotating strange stars and the data in their tables suggest that a universal maximum mass is present also for the quark-matter EOSs considered (i.e., $M_{\text{max}} \sim 1.44 M_{\text{TOV}}$), but additional work is needed to confirm this behaviour. Staykov et al. (2016) have instead considered compact stars in scalar-tensor theories and R^2 gravity, finding that relations similar to the ones reported here are valid also in such theories.

REFERENCES

- Akmal A., Pandharipande V. R., Ravenhall D. G., 1998, *Phys. Rev. C*, **58**, 1804
- Andersson N., Kokkotas K. D., 1998, *Mon. Not. R. Astron. Soc.*, **299**, 1059
- Antoniadis J., et al., 2013, *Science*, **340**, 448
- Arnett Bowers 1977, *Astrophys. J. Suppl.*, **415**, 415
- Baiotti L., Hawke I., Montero P. J., Löffler F., Rezzolla L., Stergioulas N., Font J. A., Seidel E., 2005, *Phys. Rev. D*, **71**, 024035
- Bauböck M., Berti E., Psaltis D., Özel F., *ApJ*, **777**, 68
- Bejger M., Haensel P., 2002, *Astron. Astrophys.*, **396**, 917
- Benhar O., Ferrari V., Gualtieri L., 2004, *Phys. Rev. D*, **70**, 124015
- Benhar O., Ferrari V., Gualtieri L., Marassi S., 2005, *Phys. Rev. D*, **72**, 044028
- Bernuzzi S., Nagar A., Balmelli S., Dietrich T., Ujevic M., 2014, *Phys. Rev. Lett.*, **112**, 201101
- Bhattacharyya S., Bombaci I., Logoteta D., Thampan A., 2016, preprint (arXiv:1601.06120)
- Chakrabarti S., Delsate T., Gürlebeck N., Steinhoff J., 2014, *Phys. Rev. Lett.*, **112**, 201102
- Chatziioannou K., Yagi K., Yunes N., 2014, *Phys. Rev. D*, **90**, 064030
- Cioffi R., Siegel D. M., 2015, *Astrophys. J.*, **798**, L36
- Demorest P. B., Pennucci T., Ransom S. M., Roberts M. S. E., Hessels J. W. T., 2010, *Nature*, **467**, 1081
- Doneva D. D., Yazadjiev S. S., Staykov K. V., Kokkotas K. D., 2014a, *Phys. Rev. D*, **90**, 104021
- Doneva D. D., Yazadjiev S. S., Stergioulas N., Kokkotas K. D., 2014b, *Astrophys. J. Letters*, **781**, L6
- Douchin F., Haensel P., 2001, *Astron. Astrophys.*, **380**, 151
- Falcke H., Rezzolla L., 2014, *Astron. Astrophys.*, **562**, A137
- Friedman J. L., Ipser J. R., Sorkin R. D., 1988, *Astrophys. J.*, **325**, 722
- Gaitanos T., Di Toro M., Typel S., Baran V., Fuchs C., Greco V., Wolter H. H., 2004, *Nuclear Physics A*, **732**, 24
- Gulminelli F., Raduta A. R., 2015, *Phys. Rev. C*, **92**, 055803
- Hartle J. B., 1967, *Astrophys. J.*, **150**, 1005
- Hartle J. B., 1973, *Astrophysics and Space Science*, **24**, 385
- Hartle J. B., Thorne K. S., 1968, *Astrophys. J.*, **153**, 807
- Haskell B., Cioffi R., Pannarale F., Rezzolla L., 2014, *Mon. Not. R. Astron. Soc. Letters*, **438**, L71
- Hempel, M. and Schaffner-Bielich, J. 2010, *Nucl. Phys. A*, **837**, 210

Hessels J. W., Ransom S. M., Stairs I. H., Freire P. C., Kaspi V. M., Camillo F., 2006, *Science*, 311, 1901

Kleihaus B., Kunz J., Mojica S., 2014, *Phys. Rev. D*, 90, 061501

Kramer M., Wex N., 2009, *Class. Quantum Grav.*, 26, 073001

Lasky P. D., Haskell B., Ravi V., Howell E. J., Coward D. M., 2014, *Phys. Rev. D*.

Lasota J.-P., Haensel P., Abramowicz M. A., 1996, *Astrophys. J.*, 456, 300

Lattimer J., 2015, private communication

Lattimer J. M., Prakash M., 2001, *Astrophys. J.*, 550, 426

Lattimer J. M., Schutz B. F., 2005, *Astrophys. J.*, 629, 979

Lattimer J. M., Swesty F. D., 1991, *Nucl. Phys. A*, 535, 331

Lau H. K., Leung P. T., Lin L. M., 2010, *Astrophys. J.*, 714, 1234

Majumder B., Yagi K., Yunes N., 2015, *Phys. Rev. D*, 92, 024020

Martinon G., Maselli A., Gualtieri L., Ferrari V., 2014, *Phys. Rev. D*, 90, 064026

Maselli A., Cardoso V., Ferrari V., Gualtieri L., Pani P., 2013, *Phys. Rev. D*, 88, 023007

Pandharipande Smith 1975, *Phys. Lett.*, 59B, 15

Pani P., Berti E., 2014, *Phys. Rev. D*, 90, 024025

Pappas G., Apostolatos T. A., 2014, *Phys. Rev. Lett.*, 112, 121101

Radice D., Rezzolla L., Kellerman T., 2010, *Class. Quantum Grav.*, 27, 235015

Ravenhall D. G., Pethick C. J., 1994, *Astrophys. J.*, 424, 846

Read J. S., et al., 2013, *Phys. Rev. D*, 88, 044042

Rezzolla L., Kumar P., 2015, *Astrophys. J.*, 802, 95

Rezzolla L., Zanotti O., 2013, *Relativistic Hydrodynamics*. Oxford University Press, Oxford, UK, doi:10.1093/acprof:oso/9780198528906.001.0001

Schiffrin J. S., Wald R. M., 2014, *Class. Quantum Grav.*, 31, 035024

Sham Y.-H., Chan T. K., Lin L.-M., Leung P. T., 2015, *Astrophys. J.*, 798, 121

Shen G., Horowitz C. J., Teige S., 2010, *Physical Review C*, 82, 015806

Staykov K., Doneva D., Yazadjiev S., 2016, preprint (arXiv:1602.00504v2)

Stein L. C., Yagi K., Yunes N., 2014, *Astrophys. J.*, 788, 15

Stergioulas N., Friedman J. L., 1995, *Astrophys. J.*, 444, 306

Takami K., Rezzolla L., Yoshida S., 2011, *Mon. Not. R. Astron. Soc.*, 416, L1

Takami K., Rezzolla L., Baiotti L., 2014, *Phys. Rev. Lett.*, 113, 091104

Takami K., Rezzolla L., Baiotti L., 2015, *Phys. Rev. D*, 91, 064001

Thornton D., et al., 2013, *Science*, 341, 53

Typel S., Röpke G., Klähn T., Blaschke D., Wolter H. H., 2010, *Phys. Rev. C*, 81, 015803

Urbanec M., Miller J. C., Stuchlík Z., 2013, *Mon. Not. R. Astron. Soc.*, 433, 1903

Wiringa R. B., Fiks V., Fabrocini A., 1988, *Phys. Rev. C*, 38, 1010

Yagi K., Yunes N., 2013a, *Phys. Rev. D*, 88, 023009

Yagi K., Yunes N., 2013b, *Science*, 341, 365

Yagi K., Kyutoku K., Pappas G., Yunes N., Apostolatos T. A., 2014a, *Phys. Rev. D*, 89, 124013

Yagi K., Stein L. C., Pappas G., Yunes N., Apostolatos T. A., 2014b, *Phys. Rev. D*, 90, 063010

Zhang B., 2014, *Astrophys. J.*, 780, L21

Zhang B., Mészáros P., 2001, *Astrophys. J.*, 552, L35

APPENDIX A: ANALYTICAL ESTIMATION OF THE ERROR ON THE RADIUS

As discussed in Sec. 5, we reported in Fig. 5 the relative error of the radius estimate, $\Delta R/R$, as computed numerically for the LS fit (dashed lines) and for the BR fit (continuous lines). As first pointed out by the referee, an analytical expression for the LS fit can also be obtained under a number of simplifying assumptions. To obtain such an expression, we first express the moment of inertia as [cf., Eq. (19)]

$$I = MR^2 (\tilde{a}_0 + \tilde{a}_1 \mathcal{C} + \tilde{a}_4 \mathcal{C}^4) = MR^2 \gamma, \quad (\text{A1})$$

so that $I = I(M, R, \tilde{a}_0, \tilde{a}_1, \tilde{a}_4) = I(x^j)$, where we have indicated with x^j the various degrees of freedom. The error in the measure of I can be expressed as

$$\Delta I = \left[\sum_j \left(\frac{\partial I}{\partial x^j} \right)^2 (\Delta x^j)^2 \right]^{1/2}. \quad (\text{A2})$$

Assuming $\Delta M = 0 = \Delta \tilde{a}_1 = \Delta \tilde{a}_4$, as in Lattimer & Schutz (2005), the error in the moment of inertia is

$$\Delta I = \left[\left(\frac{\partial I}{\partial \tilde{a}_0} \right)^2 (\Delta \tilde{a}_0)^2 + \left(\frac{\partial I}{\partial R} \right)^2 (\Delta R)^2 \right]^{1/2}. \quad (\text{A3})$$

We can evaluate the two terms in (A3) and obtain

$$\frac{\partial I}{\partial \tilde{a}_0} = MR^2 = \frac{I}{\gamma}, \quad (\text{A4})$$

and

$$\frac{\partial I}{\partial R} = MR \left(2\gamma + R \frac{\partial \gamma}{\partial R} \right). \quad (\text{A5})$$

A bit of algebra leads to

$$\frac{\partial \gamma}{\partial R} = -\frac{\mathcal{C}}{R} (\tilde{a}_1 + 4\tilde{a}_4 \mathcal{C}^3), \quad (\text{A6})$$

so that expression (A5) can be written as

$$\frac{\partial I}{\partial R} = MR (2\tilde{a}_0 + \tilde{a}_1 \mathcal{C} - 2\tilde{a}_4 \mathcal{C}^4) = \tilde{a}_0 MR \tilde{\chi}, \quad (\text{A7})$$

where

$$\tilde{\chi} := 2 + \frac{\tilde{a}_1}{\tilde{a}_0} \mathcal{C} - \frac{2\tilde{a}_4}{\tilde{a}_0} \mathcal{C}^4. \quad (\text{A8})$$

Using now (A4) and (A7), we rewrite (A3) as

$$\Delta I = \tilde{a}_0 MR^2 \left[\left(\frac{\Delta \tilde{a}_0}{\tilde{a}_0} \right)^2 + \tilde{\chi}^2 \left(\frac{\Delta R}{R} \right)^2 \right]^{1/2}. \quad (\text{A9})$$

Recognising now that the first term on the right-hand side of (A9) is

$$\tilde{a}_0 MR^2 = \frac{\tilde{a}_0 I}{\gamma} = \frac{I}{\chi}, \quad (\text{A10})$$

or, equivalently, that

$$\chi = 1 + \frac{\tilde{a}_1}{\tilde{a}_0} \mathcal{C} + \frac{\tilde{a}_4}{\tilde{a}_0} \mathcal{C}^4, \quad (\text{A11})$$

can rewrite it as

$$\frac{\Delta I}{I} = \frac{1}{\chi} \left[\left(\frac{\Delta \tilde{a}_0}{\tilde{a}_0} \right)^2 + \tilde{\chi}^2 \left(\frac{\Delta R}{R} \right)^2 \right]^{1/2}, \quad (\text{A12})$$

so that

$$\frac{\Delta R}{R} = \frac{1}{\tilde{\chi}} \left[\chi^2 \left(\frac{\Delta I}{I} \right)^2 - \left(\frac{\Delta \tilde{a}_0}{\tilde{a}_0} \right)^2 \right]^{1/2}. \quad (\text{A13})$$

We can next assume that the fitting error in the \tilde{a}_0 is also very small, so that $\Delta\tilde{a}_0/\tilde{a}_0 \sim 0$ and thus Eq. (A13) can be simply written as

$$\frac{\Delta R}{R} \sim \frac{\chi}{\tilde{\chi}} \frac{\Delta I}{I} = f(\mathcal{C}) \frac{\Delta I}{I}, \quad (\text{A14})$$

where the function $f(\mathcal{C})$ is defined as

$$f(\mathcal{C}) := \frac{\chi}{\tilde{\chi}} = \frac{1 + (\tilde{a}_1/\tilde{a}_0)\mathcal{C} + (\tilde{a}_4/\tilde{a}_0)\mathcal{C}^4}{2 + (\tilde{a}_1/\tilde{a}_0)\mathcal{C} - 2(\tilde{a}_4/\tilde{a}_0)\mathcal{C}^4}, \quad (\text{A15})$$

so that, once a value for the moment of inertia is fixed, expressions (19) and (A15) can be written as a function of the mass M only. A similar procedure can be carried out for the fitting in Eq. (20).

The behaviour of the denominator in the function $f(\mathcal{C})$ shows that the error can diverge for a given value of the compactness. For Eq. (A15), which is only a first approximation since it neglects the error in the moment of inertia due to the spread in the EOSs, this divergence occurs at $\mathcal{C} \sim 0.554$ when using the coefficients in Eq. (19). However, in the fully numerical analysis carried out in Fig. 5, this divergence takes place at smaller compactnesses and around $\mathcal{C} \sim 0.255$. We also note that because $f(\mathcal{C})$ depends on the compactness, there will be different relative errors $\Delta R/R$ for different choices of the moment of inertia, as shown in Fig. 5.